Geophysical Research Letters

RESEARCH LETTER
10.1029/2019GL083639

Homogenized Water Vapor Absorption Band Radiances From International Geostationary Satellites

Zhenglong Li[1], Jun Li[1], Mathew Gunshor[1], Szu-Chia Moeller[1], Timothy J. Schmit[2], Fangfang Yu[3], and Will McCarty[4]

[1]Cooperative Institute for Meteorological Satellite Studies, University of Wisconsin-Madison, Madison, WI, USA, [2]Center for Satellite Applications and Research, NESDIS/NOAA, Madison, WI, USA, [3]Earth System Science Interdisciplinary Center, University of Maryland, College Park, MD, USA, [4]Global Modeling and Assimilation Office, NASA Goddard Space Flight Center, Greenbelt, MD, USA

Abstract In the past 20+ years, GEO Imagers with infrared 6.5-μm bands have been observing the Earth's atmosphere, providing useful information of upper tropospheric moisture. Due to the instrumental differences and local viewing angles in GEO satellites, these observations are not consistent for generating climate data records (CDRs). In this study, a methodology has been developed to homogenize the 6.5-μm radiances from the international GEO satellites, to generate a consistent CDR. Validations with Infrared Atmospheric Sounding Interferometer radiances from Metops for 2015–2017 for seven GEO Imager sensors show that the GEO radiances are homogenized well with small standard deviation and biases of the differences (smaller for newer sensors), temporally stable radiometric accuracy, and weak angle dependency (even weaker for sensors with two water vapor bands). The homogenized 20+ years of consistent 6.5-μm radiance CDR can be used to evaluate reanalysis and climate models, especially the diurnal variation of the model simulation.

Key Points:
- Methodologies have been developed for consistent water vapor absorption infrared band radiances from multi-instrument/multiplatform geostationary (GEO) satellites
- Consistent water vapor absorption infrared band radiances from GEO satellites as a climate data record (CDR) have been developed and validated; they are available for climate studies and model validation
- The methodologies and technical approaches can be applied to reprocess historical satellite data for consistent CDR and current GEO data in near real time for weather applications

Supporting Information:
- Supporting Information S1

Correspondence to:
J. Li,
jun.li@ssec.wisc.edu

Citation:
Li, Z., Li, J., Gunshor, M., Moeller, S.-C., Schmit, T. J., Yu, F., & McCarty, W. (2019). Homogenized water vapor absorption band radiances from international geostationary satellites. *Geophysical Research Letters*, *46*, 10,599–10,608. https://doi.org/10.1029/2019GL083639

Received 7 DEC 2018
Accepted 13 AUG 2019
Accepted article online 21 AUG 2019
Published online 4 SEP 2019

1. Introduction

Extreme events such as droughts and floods are often associated with anomalous atmospheric conditions, including changes in mid–upper tropospheric humidity (UTH) fields (Dai, 2011), however, reliable humidity observations in the free troposphere, especially in the mid–upper troposphere, are sparse, as long-term records of radiosonde measurements often contain large biases and spurious changes (Soden, 1998). Studies (Jiang et al., 2012 and Tian et al., 2013) show that the largest model error in simulating humidity by reanalysis and climate models is in UTH. Therefore, the global water vapor (WV) observations are needed for reanalysis and climate model evaluation in order to make the projections of future global change creditable, and such WV observations can only be obtained by satellites.

Since 1994, the imagers onboard international GEO satellites, such as the U.S. Geostationary Operational Environmental Satellite (GOES and GOES-R) series (Menzel & Purdom, 1994; Schmit et al., 2005; Schmit et al., 2017), Multifunctional Transport Satellite-2 (MTSAT-2) and AHI (Advanced Himawari Imager) on Japanese Himawari series (Bessho et al., 2016; Miyamura, 2007), and Spinning Enhanced Visible and InfraRed Imager (SEVIRI) on European Meteosat Second Generation series (Schmetz et al., 2002) have provided hourly to 3-hourly (10–15 min for SEVIRI, AHI, and the Advanced Baseline Imager, ABI) infrared (IR) 6.5-μm WV absorption band radiance measurements (referred to as WV radiances in this paper). Those radiance measurements with 2- to 8-km spatial resolution from the international GEO constellation has a decent coverage of tropics and midlatitudes and can be used to assess the quality of reanalysis data sets such as Modern Era-Retrospective Analysis for Research and Analysis and Modern Era-Retrospective Analysis for Research and Analysis Version 2 (Rienecker et al., 2011), and Climate Forecast System Reanalysis (Saha et al., 2010), ECMWF Re-Analysis (ERA-40, ERA Interim; Dee et al., 2011), and climate models such as Coupled Model Inter-comparison Project Phase 5 and 6 (Taylor et al., 2012) on simulating the UTH fields associated with extreme climate events.

However, due to the instrumental (spectral response) and viewing angle differences among different sensors, there are discontinuities in the global WV radiance imagery from the international GEO constellation, especially in the overlapping area. That greatly hinders the climate applications of those WV radiance observations. In this study, a homogenization methodology has been developed to generate a consistent WV

Table 1
Location, Center Wavelength of Spectral Bands Used in Homogenization (Water Vapor Bands in Bold), Launch Year, Satellite Subpoint Spatial Resolution, and Time Coverage of the Seven International Geostationary Imagers for the Time Period of 2015–2017

Sensor	GEO satellite	Position (longitude)	WV bands (μm)	Launch year	Spatial resolution	Time coverage
G13I	GOES-13	−75°	**6.5**, 10.7, 13.3	2006	4 km	1/2015 to 12/2017
G15I	GOES-15	−135°	**6.5**, 10.7, 13.3	2010	4 km	1/2015 to 12/2017
AHI8	Himawari-8	140.68°	**6.2**, **6.9**, 11.2, 13.3	2014	2 km	3/2015 to 12/2017
SEVIRI10	Meteosat-10 (MSG3)	9.5°	**6.2**, **7.35**, 10.8, 13.4	2012	3 km	1/2015 to 12/2017
SEVIRI08	Meteosat-8 (MSG1)	41.5°	**6.2**, **7.35**, 10.8, 13.4	2002	3 km	10/2016 to 12/2017
ABI16	GOES-16	−89.5° or −75.2°	**6.2**, **6.9**, 11.2, 13.3	2016	2 km	7/2017 to 12/2017
MTSAT-2	MTSAT-2 (Himawari-7)	145°	**6.75**, 10.8, 12.0	2006	4 km	1/2015 to 11/2015

Note. GOES-16 was moved to −75.2°W in mid-December 2017. G13I = GOES-13 Imager; G15I = GOES-15 Imager; GOES = Geostationary Operational Environmental Satellite; AHI = Advanced Himawari Imager; SEVIRI = Spinning Enhanced Visible and InfraRed Imager; ABI = Advanced Baseline Imager; MTSAT-2 = Multifunctional Transport Satellite-2.

radiance climate data record (CDR) from the international GEO satellites. The homogenization process converts all other GEO Imager WV radiances to GOES-15 Imager (G15I) 6.5-μm band nadir view radiances. A simple cloud mask scheme is implemented in postprocessing to remove observations affected by clouds. Comparisons between Infrared Atmospheric Sounding Interferometer (IASI; Blumstein et al., 2007) and seven GEO Imager sensors (GOES-13 Imager [G13I], G15I, SEVIRI onboard Meteosat-8/Meteosat-10, AHI onboard Himawari-8 [AHI8], MTSAT-2 Imager onboard Himawari-7, and ABI onboard GOES-16 [ABI16]) from 3 years (2015-2017) show reasonable standard deviation (STD) and biases of the differences of the homogenized GEO radiances, with newer sensors having better results than older ones. The stable daily time series of G13I, G15I, AHI8, and SEVIRI10 biases over the 3 years indicate that the homogenization process does not change radiometric stability. The homogenization shows weak angle dependency, however, the angle dependency is not as substantial for sensors with two WV bands (e.g., SEVIRI) used in the homogenization process, which provide more information about the atmosphere vertically than those with only one WV band. This homogenization process will ensure interconsistency between different GEO satellites with good accuracy for capturing the atmospheric WV changes.

It is important to point out that global homogenized WV radiance CDR have been generated from polar orbiting satellites, such as channel 12 of the High-Resolution Infrared Radiation Sounder (Shi & Bates, 2011) and 183 ± 1 GHz from Special Sensor Microwave Water Vapor Profiler (SSM/T-2), Advanced Microwave Sounding Unit-B (AMSU-B) and Microwave Humidity Sounder (Hans et al., 2019). Data sets like those have been successfully used for climate studies (Buehler et al., 2008; Kottayil et al., 2016; Shi et al., 2012). However, due to limitations of polar orbiting satellites, such as low revisit frequency, variable equator crossing time, and orbit drifting, their applications to climate studies are somehow limited, especially on diurnal variations. The homogenized WV radiance CDR from international GEO imagers, on the other hand, is able to fill the temporal gap and provide complementary information about UTH. Such data sets can also be used for intercomparison with polar orbiting satellite based WV radiance CDR.

2. GEO Imager Radiance Data

Three years of GEO imager data from 2015 to 2017 is used to demonstrate the methodologies in this study. Within that time period, seven GEO imagers are available: GOES-13 Imager, G15I, ABI16, AHI8, MTSAT-2, Meteosat-8/Meteosat-10 SEVIRI (SEVIRI08 and SEVIRI10). Table 1 lists some of the details of the GEO imagers. All of the sensors have a spatial resolution of 4 km or better and have at least one WV spectral band near 6.5-μm. These imagers are capable of observing the mid–upper tropospheric WV in IR spectral bands, which can be used for climate and other applications. Figure 1a illustrates the moisture Jacobians of the WV absorption bands for selected sensors using the U.S. 1976 Standard Atmosphere with a nadir view. G15I and MTSAT-2 both (G13I as well) have single WV band peaking around the same height near 350 hPa, while SEVIRI10 (SEVIRI08 as well) has two WV absorption bands with one peaking higher and the other lower than the G15I WV band. ABI16 (AHI8 as well) has three WV bands, with one higher and the other two lower than the G15I WV band. Figure 1 indicates that all other sensors either have similar or more moisture information than G15I, which is the last satellite of current GOES series; thus, G15I can be used as the benchmark

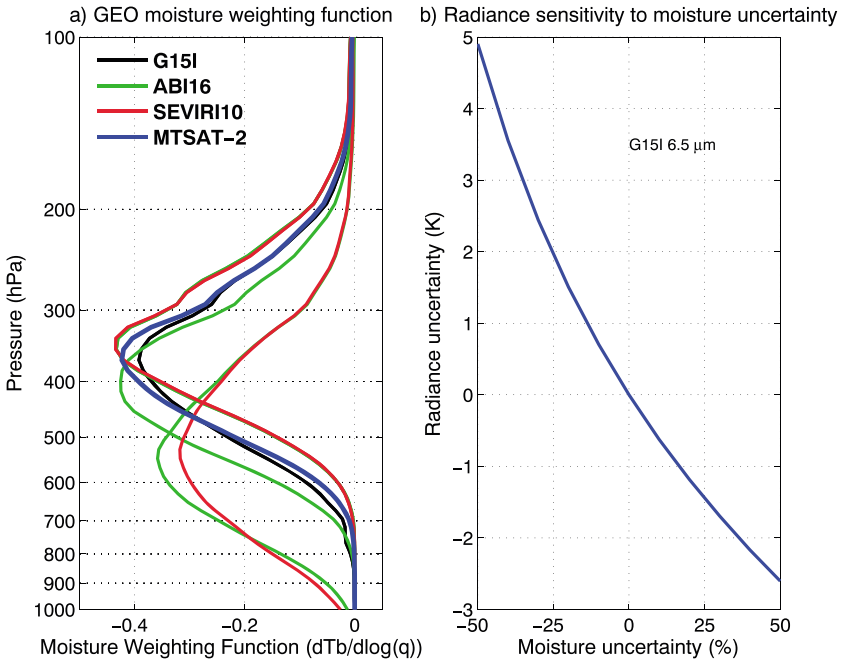

Figure 1. (a) Moisture weighting functions (Jacobians) from the water vapor bands of imagers on selected international geostationary satellites. Note that these pairs of sensors have weighting functions almost identical due to band similarity: G13I/G15I, AHI8/ABI16, and SEVIRI8/SEVIR10. (b) The simulated GOES-15 Imager 6.5-μm radiance sensitivity (in the unit of brightness temperature, K) to moisture uncertainty of the whole troposphere. The U.S. 1976 Standard Atmosphere profile with a nadir view is used in the calculations. SEVIRI = Spinning Enhanced Visible and InfraRed Imager; ABI = Advanced Baseline Imager;G13I = GOES-13 Imager; G15I = GOES-15 Imager; GOES = Geostationary Operational Environmental Satellite.

to homogenize other sensors. Although some sensors are capable of observing the full disk every 15 min (i.e., SEVIRI and ABI) or better (i.e., 10 min for AHI), the data are processed every 3 hr, to be consistent with the GOES Imager full disk frequency.

Figure 1b shows the simulated G15I 6.5-μm radiance change (in the unit of brightness temperature, K) as a function of moisture uncertainty. The Community Radiative Transfer Model (Chen et al., 2012) developed by the Joint Center for Satellite Data Assimilation of NOAA is used in all radiative transfer (RT) and Jacobian related calculations. For U.S. 1976 Standard Atmosphere, which has moderate moisture content, the WV radiance change could be as large as 5 K when WV content is reduced by 50 %. Note that the moisture change used in Figure 1b is the relative change of water vapor content (mixing ratio) of the whole troposphere, not the change of relative humidity. With relative humidity, a decrease of 50% may result in even larger radiance change. This is also true for more moist atmospheres, such as tropics and midlatitude summer. On the other hand, for a WV radiance change of 5 K, a temperature change of about 5.6 K would be needed, which is unlikely for the troposphere in these model simulations. Therefore, when using the satellite WV absorption band radiance observations for evaluating the climate model performance, large differences between observations and calculations may be considered primarily from moisture uncertainty in the model.

The data used in this study are provided by the Space Science and Engineering Center Data Center, which currently archives research quality data from nine different geostationary satellites including all GOES (Menzel & Purdom, 1994), Himawari (Bessho et al., 2016), and Meteosat (Schmetz et al., 2002).

3. Methodologies

The purpose of this study is to generate a consistent CDR from international GEO imagers. More specifically, all other sensors' WV radiance observations will be homogenized and converted to nadir view of G15I 6.5-μm. There are two major differences between other sensors and nadir view G15I: spectral differences and angle differences, while the G15I only has angle difference compared with its nadir view. The

spectral differences are caused by the differences in SRFs, while the angle differences are caused by the local zenith angle differences. The homogenization process is one single step performing both spectral and limb (angular) adjustments using a simple linear regression approach:

$$y = XK \tag{1}$$

where y is a scalar, the predicted G15I 6.5-μm brightness temperature (Tb) at nadir view, K is the vector of the regression coefficients, and X is the vector of the predictors, which are the Tb of selected spectral bands. Note that while it makes sense to take two steps (spectral and limb) of adjustments, simulation study shows no additional benefits of two steps over the single step adjustment. A spectral band is considered useful in the homogenization process if it provides atmosphere information about the would-be G15I 6.5-μm. The primary predictors are WV radiance observations. For G13I, G15I, and MTSAT-2, there is only one single WV band and it is used as the primary predictor, which happens to be similar to G15I 6.5-μm. For ABI, AHI, and SEVIRI, two WV bands are used as primary predictors with one above and the other below G15I 6.5-μm (see Table 1 for bands used as predictors). For all sensors, it is preferred to have CO_2 spectral bands included as supplemental predictors to provide atmospheric temperature information. Since there is only one CO_2 band around 13.3-μm on any of the imagers, it is included as a predictor. The sensitivity test using the training data set shows that the STD of SEVIRI10's homogenized WV radiance uncertainty is significantly increased by 18 %, or the variance by 40% without the CO_2 band. MTSAT-2 has no CO_2 band, so the 12.0-μm dirty window band is used instead. Lastly, one clean window band around 10.8-μm is included as one additional supplemental predictor. This band is more sensitive to clouds than WV and CO_2 bands, especially when clouds are lower than the peaking heights of those absorption bands. The predicted G15I 6.5-μm radiance will have increased sensitivity to clouds than original WV radiances. This will make cloud screening easier in postprocessing.

The SeeBor database (Seemann et al., 2008) is used to generate the training dataset for regression. For all of the 15,704 profiles, Community Radiative Transfer Model 2.1.3 with Optical Depth in Pressure Space coefficients is used for forward RT calculation with 11 local zenith angles (LZAs): 0.0°, 24.62°, 33.56°, 39.72°, 44.42°, 48.19°, 51.32°, 53.97°, 56.25°, 58.24°, and 60.0°. This classification is selected so that their secant values are evenly distributed. With this angle classification, the secant value of LZA is found to add no additional value in the homogenization process and thus is not used as a predictor. To ensure the accuracy of RT calculation, the forward RT calculation is only performed for IASI/Metop-A. Operational SRFs are used to generate radiances for each of the sensors from the simulated IASI/Metop-A radiances. Gaussian distributed random numbers based on each sensor's in-orbit noise equivalent delta temperature, or NEdT, are generated to simulate observation noise (Li et al., 2018, 2019). Linear regression coefficients are generated for each of the 10 non-zero LZA classes. In application for any given zenith angle, coefficients from the two nearest zenith classes will be chosen. Weighted average of the two adjustments will provide the limb and spectrally adjusted Tb.

A simple cloud mask scheme based on radiance observations is implemented in the postprocessing. The 6.5-μm band is sensitive to the upper troposphere, where both the moisture and temperature fields are generally smooth in spatial distribution. The cloud detection focuses on high clouds using two criteria: (a) the brightness temperature difference between a low peaking band (i.e., the clean window band) and a high peaking band (i.e., the WV band) should be large in clear sky, and (b) cloud regions are not as homogeneous as clear regions. The first criterion is applied to the original radiance measurements, and the second one is applied to the homogenized Tb. These two criteria together should be able to effectively remove 6.5-μm band observations affected by clouds.

For each sensor and each angle classification, the F value and p value are examined to ensure the overall significance of the linear regression model; all sensors and angles are found to have F values larger than 150,000 and p values of 0. The regression coefficients are provided in the supporting information.

4. Results

The methodology introduced in the previous section is applied to process the 3 years of GEO radiance data from 2015 to 2017. During the three years, seven GEO imager sensors are processed, including G13I, G15I,

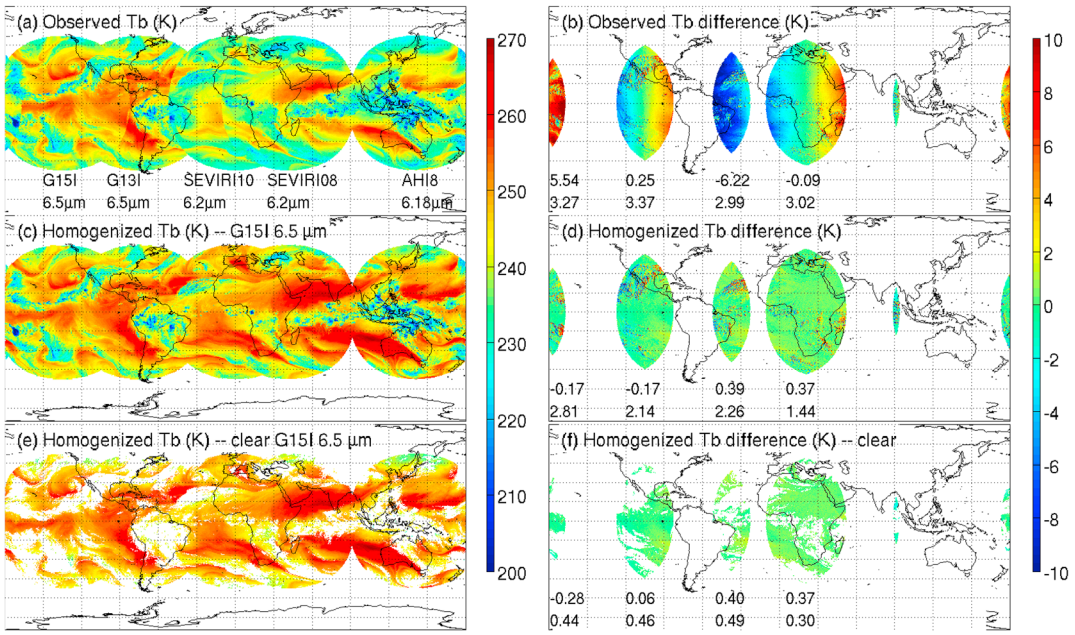

Figure 2. An example of global water vapor radiance observations (a) before, (c) after the homogenization, and (e) after the homogenization in clear skies at 06 UTC on 30 December 2016. Panels (b), (d), and (f) show imagery differences in the overlapping areas between two nearby sensors (the east minus west). The numbers below each overlapping area shows the mean (first row) and standard deviation (second row) of difference. The overlapping area between SEVIRI08 and AHI8 is too small to have enough sample for statistics. G13I = GOES-13 Imager; G15I = GOES-15 Imager; GOES = Geostationary Operational Environmental Satellite; AHI = Advanced Himawari Imager; SEVIRI = Spinning Enhanced Visible and InfraRed Imager.

ABI16, AHI8, MTSAT-2, SEVIRI08, and SEVIRI10. The methodology can be applied to process the 20+ years of GEO radiance data following the same technical approaches.

4.1. Case Demonstration

Figure 2 shows a randomly selected example from 06 UTC on 30 December 2016. At this time, there are five sensors available: G13I, G15I, AHI8, SEVIRI08, and SEVIRI10. Figure 2a shows the original WV radiance measurements from the five sensors. For sensors with more than one WV band, the highest peaking band is shown. Even though the radiances are limited to LZA of less than 60°, the five sensors together have a decent coverage of tropics and midlatitudes with overlapping between adjacent satellites. In the overlapping area, it is clear that there exist discontinuities. As pointed out before, these discontinuities are caused by the SRF and LZA differences. For example, Figure 2b shows SEVIRI10 is 6.22 K colder than G13I, and G15I is 5.54 K warmer than AHI8 in overlapping area. That is because the WV bands from AHI8 and SEVIRI10 peak higher (SRF differences) than the 6.5-μm band from G13I and G15I. Figure 2b also shows that the mean differences between the two GOES Imagers and the two SEVIRIS are close to 0, indicating the similarity between those pairs. The strong gradients between those pairs are caused by the LZA differences.

From Figure 2c, the homogenization process warms up almost all the observations. This is reasonable because the observations are converted to have a nadir view now. Also, for AHI8 and the two SEVIRIs, the 6.5-μm peaks lower than the original bands shown in Figure 2a. More importantly, the homogenization successfully removes those discontinuities in the overlapping area. This is more evident on the difference (east sensor minus west sensor) imagery. Figure 2d shows that the homogenization process brings the imagery differences close to zero except over clouds. These results indicate that the homogenization process is able to remove the differences caused by SRF and LZA differences and make the observations from different sensors consistent with each other, although this is only true in clear sky conditions. In cloudy regions, from Figure 2d, the homogenization does not work well because all the coefficients are derived in clear sky only. To evaluate the effectiveness of cloud detection, the homogenized clear sky radiances are shown in Figure 2 e, and the difference imagery in Figure 2f. On both figures, the impacts of clouds are not evident. And the

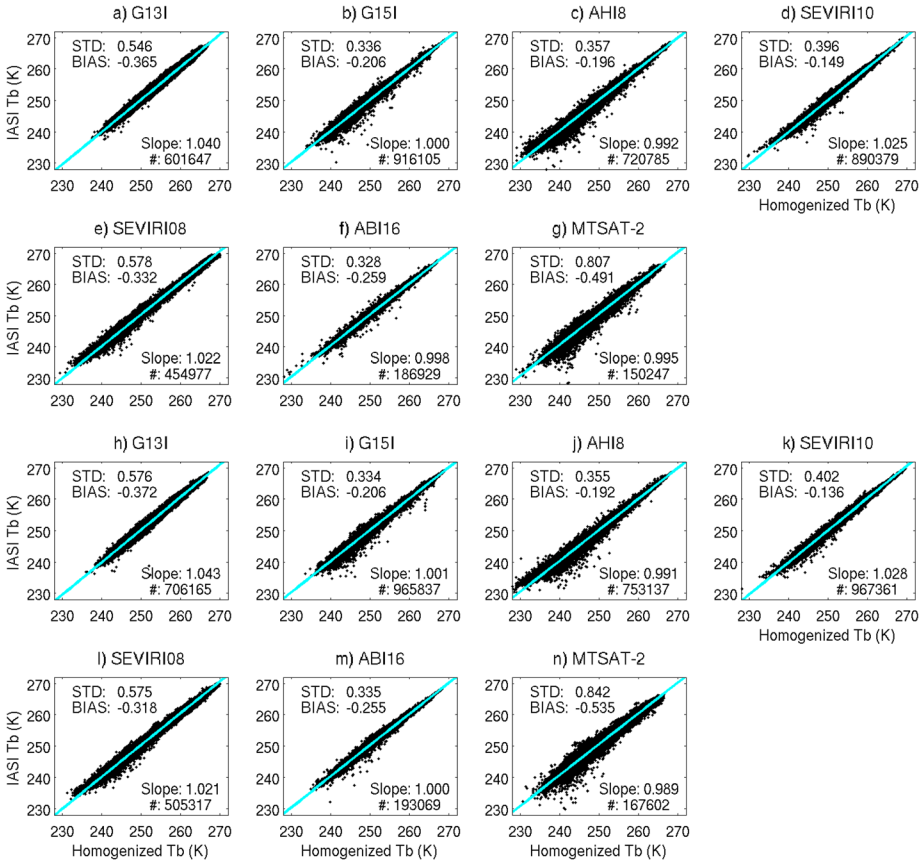

Figure 3. Scatter plots of radiances (K) between the homogenized 6.5-μm GEO imagers and IASI for 2015–2017 along with statistics of standard deviation (STD), biases of differences, and slope. Panels (a)–(g) use IASI/Metop-A as reference, and panels (h)–(n) use IASI/Metop-B as reference. The number of collocated observations is also shown. G13I = GOES-13 Imager; G15I = GOES-15 Imager; GOES = Geostationary Operational Environmental Satellite; AHI = Advanced Himawari Imager; SEVIRI = Spinning Enhanced Visible and InfraRed Imager; ABI = Advanced Baseline Imager; MTSAT-2 = Multifunctional Transport Satellite-2; IASI = Infrared Atmospheric Sounding Interferometer.

STD of differences are greatly reduced once the clouds are removed. These results indicate that the homogenization process works well in clear sky and the cloud mask algorithm successfully removes the cloudy pixels.

4.2. Validation With IASI

IASI radiances are used to validate the homogenized GEO WV radiances. IASI radiances on both Metop-A and Metop-B are convolved with G15I SRF to generate G15I 6.5-μm radiances with IASI viewing geometry. This is a similar concept to the Global Space-based Inter-Calibration System (GSICS) GEO-LEO intercalibration, but different methodology, primarily in that GSICS uses stricter criteria for matching pixels (Hewison et al., 2013). Since the homogenized WV data set is 3-hourly, looser restrictions on pixel matching to IASI are justified in order to generate enough comparisons. The GEO WV band radiances are temporally and spatially interpolated (linearly) to IASI grids. The IASI-GEO time differences are smaller than 15 min, and the IASI LZA is less than 10° for comparisons. Figure 3 shows the scatter plots for the seven sensors processed. For both IASIs, all the seven sensors show good agreement in terms of STD and biases of the Tb differences. All recent sensors (see Table 1 for launch year), such as G15I, AHI8, SEVIRI10, and ABI16, have great agreements with IASIs; the absolute biases are less than 0.26 K, and STDs are less than 0.41 K. G13I, and SEVIRI08, launched in 2006 and 2002 respectively, have slightly larger but still reasonable biases (better than 0.38 K for absolute biases) and STD (better than 0.58 K). The MTSAT-2 has the worst statistics out of all seven sensors; the biases are around −0.5 K and STDs a little over 0.8 K. It is important to point out that similar agreement in terms of biases could be obtained if relaxing the collocation criteria, such as the time

difference and IASI LZA, but the STDs will be slightly increased. These results indicate that the homogenization process is able to spectrally convert the original GEO WV radiances from different international GEO satellites to G15I nadir view. It is interesting to note that G15I and AHI8 appear to be more scattered than G13I, but with much smaller STDs. The density scatter plot (not shown) shows that most data of G15I and AHI8 are along the regression line, which means they are less scattered.

Compared with the original WV radiances, the homogenized WV radiances have combined information from multiple bands. Although this homogenization is to adjust the original radiances from all GEO satellites to G15I spectral response, it does not dramatically change the overall instrument radiometric accuracy. The GSICS program offers an opportunity to examine the GEO instrument radiometric accuracy. For example, SEVIRI10 has overall biases slightly above −0.2 K for 6.2-μm from 2015 to 2017, when compared with IASI/Metop-A. Figure 3 shows that the homogenized 6.5-μm radiances have an overall bias slightly above −0.15 K compared with both IASIs, which indicates that the homogenization does not dramatically change the overall radiometric accuracy of the homogenized 6.5-μm radiances from the original SEVIRI10 radiances. Hewison et al. (2013) shows that MTSAT-2 has biases of −0.25 K for 6.75-μm band from summer 2010 to fall 2012, which has been stable until early 2016 according to the GSICS website. The homogenized WV radiances from MTSAT-2 have a relatively large bias about −0.5 K from January 2015 to November 2015. The larger biases from larger LZA is due to the increased difficulty of limb adjustment as shown in the lower panel of Figure 4: the mean bias is −0.70 K for LZA larger than 40° and −0.37 K for LZA smaller than 40°.

It is important to ensure that the homogenization does not dramatically change the temporal radiometric stability. The upper panel of Figure 4 shows the daily time series of radiance biases for four of the homogenized sensors using IASIs as reference as well as the trend with 95% confidence interval, the F values, and p values. These four sensors are chosen because they have data for almost the whole 3 years. Every point in the upper panel of Figure 4 represents the mean bias for the nearby 2 weeks (1 week before and 1 week after) to account for the daily small sample size due to the strict collocation conditions (15-min time difference and IASI LZA less than 10°). From the upper panel of Figure 4, while it is difficult to see the trends visually, the calculation does show some trends compared with IASIs. SEVIRI10 has the strongest trend among the four sensors: a statistically significant warming trend slightly less than 0.05 K/year. This warming trend is likely due to the increased biases in the 13.4-μm CO_2 band caused by ice built up on the optics of SEVIRI (Hewison & Müller, 2013). After removing 2017, the trend becomes insignificant. For G13I and G15I, there is no conclusive evidence that the two sensors have statistical significant trends, because one IASI shows significant trend with extremely small p values and large F values, while the other shows insignificant trend with large p values and small F values. AHI8, on the other hand, shows significant cooling trends of about −0.016 K/year from both IASIs. This cooling trend is not due to the homogenization process because similar cooling trends are presented in the GSICS monitoring by JMA at http://www.data.jma.go.jp/mscweb/data/monitoring/gsics/ir/monit_geoleoir.html website. Such a small trending between IASIs and AHI8 indicates that the radiance of these three instruments are all well calibrated and very stable during the study period, and the radiometric calibration of the AHI8 is more stable than the legacy instruments. The results presented in Figure 4 upper panel indicate that the homogenization does not change the temporal radiometric stability.

Figure 3 also shows the slope from the linear fit between the homogenized and IASI radiances. Both AHI8 and ABI16, as the newest generation of GEO Imager, have slopes close to 1, again indicating their excellent radiometric accuracies and stabilities. SEVIRI10 and SEVIRI08 both show slopes substantially larger than 1, indicating there exist scene temperature dependent biases. This is probably due to the bias fluctuation of the 7.35-μm, as shown from the GSICS website. On the contrary, the JMA GSICS website shows that the MTSAT-2 is much more radiometrically stable. As a result, MTSAT-2 shows the slope much closer to 1 than the two SEVIRIs, despite being an old sensor with larger STD and bias. G13I shows the largest slope of the seven sensors. That is likely due to the seasonal variations of the 6.5-μm bias, as shown from the NOAA's website for GOES Imager data quality monitoring (https://www.star.nesdis.noaa.gov/smcd/spb/fwu/homepage/GOES13_Imager_DataQualityMonitoring.php). The same website also shows that G15I does not have those seasonal variations, which explains why the slope of G15I is much closer to 1.

To further examine the effectiveness of the limb correction, the validation is categorized into different GEO LZAs. The lower panel of Figure 4 shows the statistics of STD and bias for the seven GEO sensors at different GEO zenith angles binned at 5° compared with IASI/Metop-A. Results are similar when compared with

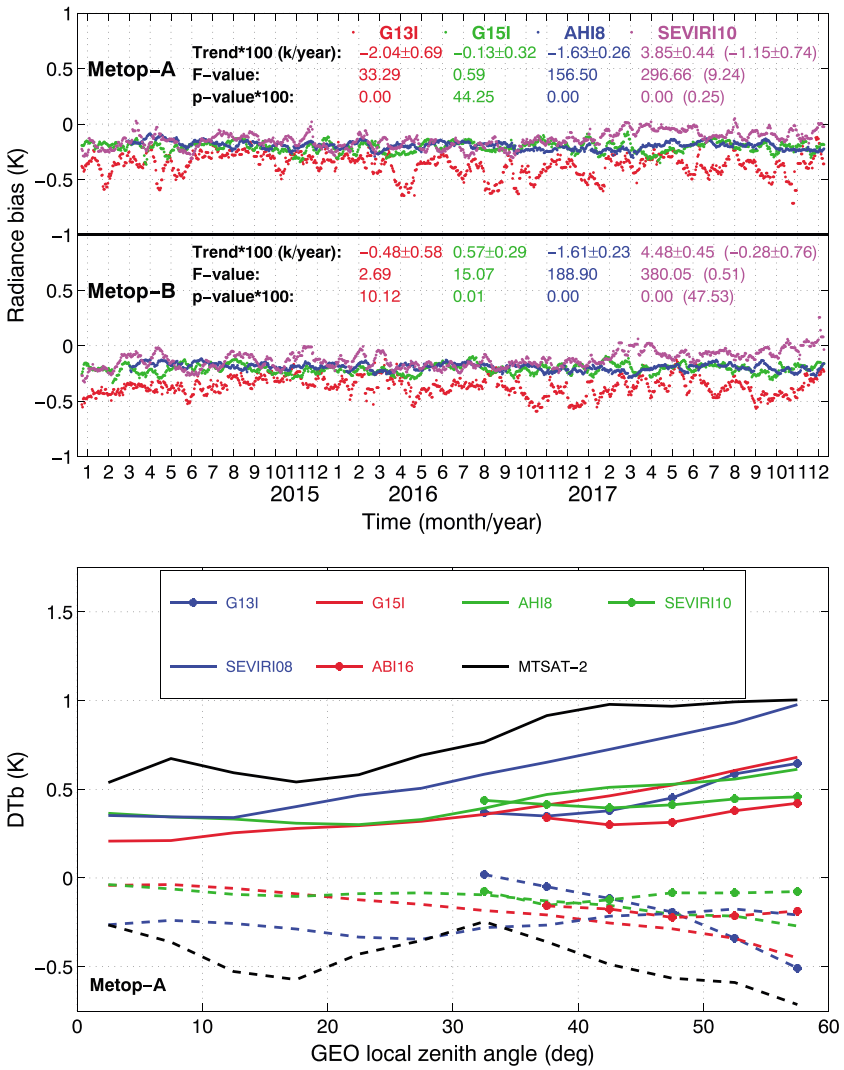

Figure 4. (upper panel) Daily time series of radiance biases (K) for the four homogenized sensors from 2015 to 2017 using the two IASI as references. Also shown are the trend * 100 in kelvins per year with a 95% confidence interval, the *F* value, and *p* value. The SEVIRI10 numbers in bracket are calculated without the warming data in 2017. (lower panel) The standard deviation (solid lines) and biases (dashed lines) of the homogenized GEO water vapor radiances using IASI/Metop-A as references as a function of GEO LZA (IASI/Metop-B shows similar results). Note G13I, SEVIRI10, and ABI16 have no collocations with IASI for LZA smaller than 30°. G13I = GOES-13 Imager; G15I = GOES-15 Imager; GOES = Geostationary Operational Environmental Satellite; AHI = Advanced Himawari Imager; SEVIRI = Spinning Enhanced Visible and InfraRed Imager; ABI = Advanced Baseline Imager; MTSAT-2 = Multifunctional Transport Satellite-2; LZA = local zenith angle; IASI = Infrared Atmospheric Sounding Interferometer.

IASI/Metop-B. The collocation criteria are relaxed to (a) time difference of 30 min and (b) IASI LZA less than 15° to increase sample size for all zenith angles. For all seven sensors, STD increases and bias decreases as zenith increases. This indicates that the limb correction becomes more difficult as the LZA increases. This angle dependency is more evident for G13I, G15I, and MTSAT-2, all of which have only one WV band. The limb correction adjusts the WV radiances as if the sensor is observing with the nadir view. For WV bands, that essentially lowers the weighting function peaking height in the vertical. Therefore, information about atmosphere below the original WV band will be helpful in the homogenization. For G13I, G15I, and MTSAT-2, only one CO_2 band (one dirty window for MTSAT-2) is used to account for the atmosphere below the WV band. The CO_2 or dirty window band peaks in the lower troposphere or near the surface, providing limited information about the atmosphere right below the WV band. That limits the effectiveness of limb correction, resulting in substantial angle dependency in both STD and bias for

those three sensors. For ABI16, AHI8, and SEVIRI10, there are two WV bands used in the homogenization, providing more needed information about the atmosphere around the 6.5-μm peak height (see Figure 1 for peak height of those WV bands). As a result, these three sensors show reduced angle dependency in both STD and bias. SEVIRI08 also has two WV bands used in the homogenization as well. However, SEVIRI08 has a larger angle dependency in STD than ABI16, AHI8, and SEVIRI10, although not very obvious in the bias. In fact, its angle dependency in STD is even larger than G13I, G15I, and MTSAT-2. That is because of the overall low radiometric stability of SEVIRI08. According to GSICS website, SEVIRI08 7.35-μm has a large bias fluctuation between 0.65 and 0.2 K from October 2016 to December 2017. And the 13.4-μm band has a very large bias fluctuation between −1.7 and 0.6 K from October 2016 to December 2017. These inherent biases substantially affect the homogenization.

Figure 4 indicates there could exist residual spatial inhomogeneity in the homogenized WV radiances, since the STD increases and the bias decreases with the zenith angle. The spatial inhomogeneity can be better seen in the supplemental version of Figures 2d and 2f, where some areas have larger differences between G13I and G15I, also between SEVIRI08 and SEVIRI10. While it is difficult to further correct such spatial inhomogeneity, it should be kept in mind when utilizing the homogenized WV radiances.

5. Summary

The central objectives of this study are to generate a data set, covering the last 20+ years, providing consistent WV absorption band (~6.5-μm) IR radiances from international GEO satellites as a CDR for climate studies, and to quantitatively assess the capability of UTH simulation for reanalysis and climate models. Methodologies and technical approaches have been developed to homogenize all other GEO Imager WV band radiances using nadir GOES-15 Imager WV band radiances as reference. This homogenization process accounts for both the limb effect and the spectral differences between other GEO imagers and GOES-15 Imager. The limb effect and spectral differences are successfully removed, and there is no obvious discontinuity between different satellites after the homogenization, which indicates the homogenization process is able to convert various geostationary imager WV radiances to a consistent database. IASI radiances from both Metop-A and Metop-B, which have full IR spectral coverage and high spectral and radiometric calibration accuracies, are used as independent references to validate the homogenized GEO WV radiances. The results show that all of the GEO WV radiances are homogenized well with small standard deviation (STD, 0.3–0.6 K except MTSAT-2 of 0.8 K) and biases (−0.14 to −0.54 K) of the differences, temporally stable radiometric accuracy, and weak angle dependency. The newer sensors, such as G15I, AHI8, SEVIRI10, and ABI16, show better statistics than old sensors with STDs less than 0.41 K and absolute biases less than 0.26 K. The sensors with two WV bands used in the homogenization, such as AHI8, SEVIRI10, and ABI16, show much weaker angle dependency than those having only one WV band, such as G13I, G15I, and MTSAT-2. SEVIRI08 has largest angle dependency in STD than other sensors because of its overall low radiometric stability.

The methodologies and technical approaches can be applied to process historical GEO satellite imager WV radiances (20+ years) for consistent CDR, and they can also be applied to process GEO imager data in near real-time for weather applications. However, it should be noted that going back to previous generation imagers such as GOES-7, Meteosat-7, and GMS-5 would need more effort, and international collaboration (e.g., very different calibration approaches and much wider spectral region; see John et al., 2019; Tabata et al., 2019) although all the data are also archived at the Space Science and Engineering Center Data Center. Future work will include the assessment of reanalysis and climate models for simulating the upper tropospheric moisture using the homogenized GEO WV radiances.

Acknowledgments
This work is partly supported by the NASA ROSE program (EOS NNH15ZDA001N-SCIS). The L1b radiance measurements from international GEO imagers and two IASIs are provided by the Data Center of Space Science and Engineering Center at University of Wisconsin-Madison (https://www.ssec.wisc.edu/datacenter/dcmain.html). The SeeBor database is available online (https://cimss.ssec.wisc.edu/training_data/). The regression coefficients and the Matlab reader have been provided in the supporting information of this manuscript and are also available online (ftp://ftp.ssec.wisc.edu/ABS/zli/GEO_WV_Homogenization_Coeffs/regression_coef_supplemental_materials.tar). The homogenized WV radiances can be obtained by applying the regression coefficients to the GEO imager radiances.

References

Bessho, K., Date, K., Hayashi, M., Ikeda, A., Imai, T., Inoue, H., et al. (2016). An introduction to Himawari-8/9—Japan's new-generation geostationary meteorological satellites. *Journal of the Meteorological Society of Japan*, *94*(2), 151–183. https://doi.org/10.2151/jmsj.2016-009

Blumstein D., Tournier, B., Cayla, F. R., Phulpin, T., Fjortoft, R., Buil, C., & Ponce, G. (2007). In-flight performance of the infrared atmospheric sounding interferometer (IASI) on Metop-A, in Proc. SPIE, 2007, vol. 6684, pp. 66840H-1–66840H-12.

Buehler, S. A., Kuvatov, M., John, V. O., Milz, M., Soden, B. J., Jackson, D. L., & Notholt, J. (2008). An upper tropospheric humidity data set from operational satellite microwave data. *Journal of Geophysical Research*, *113*, D14110. https://doi.org/10.1029/2007JD009314

Chen, Y., Han, Y., & Weng, F. Z. (2012). Comparison of two transmittance algorithms in the community radiative transfer model: Application to AVHRR. *Journal of Geophysical Research*, *117*, D06206. https://doi.org/10.1029/2011JD016656

Dai, A. (2011). Drought under global warming: A review. *Wiley Interdisciplinary Reviews: Climate Change*, *2*(1), 45–65.

Dee, D. P., Uppala, S. M., Simmons, A. J., Berrisford, P., Poli, P., Kobayashi, S., et al. (2011). The ERA-Interim reanalysis: Configuration and performance of the data assimilation system. *Quarterly Journal of the Royal Meteorological Society*, *137*(656), 553–597. https://doi.org/10.1002/qj.828

Hans, I., Burgdorf, M., Buehler, S. A., Prange, M., Lang, T., & John, V. O. (2019). An uncertainty quantified fundamental climate data record for microwave humidity sounders. *Remote Sensing*, *11*(5), 548. https://doi.org/10.3390/rs11050548

Hewison, T., & Müller, J. (2013). Ice contamination of Meteosat/SEVIRI implied by inter-calibration against Metop/IASI. *IEEE Transactions on Geoscience and Remote Sensing*, *51*(3), 1182–1186. https://doi.org/10.1109/TGRS.2012.2236335

Hewison, T. J., Wu, X., Yu, F., Tahara, Y., & Koenig, M. (2013). GSICS inter-calibration of infrared channels of geostationary imagers using Metop/IASI. *IEEE Transactions on Geoscience and Remote Sensing*, *51*(3), 1056–1080.

Jiang, J. H., Su, H., Zhai, C., Perun, V. S., Del Genio, A., Nazarenko, L. S., et al. (2012). Evaluation of cloud and water vapor simulations in CMIP5 climate models using NASA "A-Train" satellite observations. *Journal of Geophysical Research*, *117*, D14105. https://doi.org/10.1029/2011JD017237

John, V. O., Tabata, T., Rüthrich, F., Roebeling, R. A., Hewison, T., Stoeckli, R., & Schulz, J. (2019). On the methods to recalibrate geostationary longwave channels using polar orbiting infrared sounders. *Remote Sensing*, *11*, 1171. https://www.mdpi.com/2072-4292/11/10/1171/htm

Kottayil, A., John, V. O., Buehler, S. A., & Mohanakumar, K. (2016). Evaluating the diurnal cycle of upper tropospheric humidity in two different climate models using satellite observations. *Remote Sensing*, *8*(4), 325. https://doi.org/10.3390/rs8040325

Li, Z., Li, J., Schmit, T. J., Wang, P., Lim, A., Li, J., et al. (2019). The alternative of CubeSat-based advanced infrared and microwave sounders for high impact weather forecasting. *Atmospheric and Oceanic Science Letters*, *12*(2), 80–90. https://doi.org/10.1080/16742834.2019.1568816

Li, Z., Li, J., Wang, P., Lim, A., Li, J., Schmit, T. J., et al. (2018). Value-Added Impact of Geostationary Hyperspectral Infrared Sounder on Local Severe Storm Forecasts – Via a Quick Regional OSSE. *Advances in Atmospheric Sciences*, *35*(10), 1217–1230. https://doi.org/10.1007/s00376-018-8036-3.

Menzel, W. P., & Purdom, J. F. W. (1994). Introducing GOES-I: The first of a new generation of Geostationary Operational Environmental Satellites. *Bulletin of the American Meteorological Society*, *75*(5), 757–781. https://doi.org/10.1175/15

Miyamura, K. (2007). MTSAT-2 systems (in Japanese). *MSC technical note*, *49*, 55–58.

Rienecker, M. M., Suarez, M. J., Gelaro, R., Todling, R., Bacmeister, J., Liu, E., et al. (2011). MERRA—NASA's Modern-Era Retrospective Analysis for Research and Applications. *Journal of Climate*, *24*(14), 3624–3648. https://doi.org/10.1175/JCLI-D-11-00015.1

Saha, S., Moorthi, S., Pan, H. L., Wu, X., Wang, J., Nadiga, S., et al. (2010). The NCEP climate forecast system reanalysis. *Bulletin of the American Meteorological Society*, *91*(8), 1015–1058. https://doi.org/10.1175/2010BAMS3001.1

Schmetz, J., Pili, P., Tjemkes, S., Just, D., Kerkmann, J., Rota, S., & Ratier, A. (2002). An introduction to Meteosat Second Generation (MSG). *Bulletin of the American Meteorological Society*, *83*(7), 992–992. https://doi.org/10.1175/BAMS-83-7-Schmetz-2

Schmit, T. J., Griffith, P., Gunshor, M. M., Daniels, J. M., Goodman, S. J., & Lebair, W. J. (2017). A Closer Look at the ABI on the GOES-R Series. *Bulletin of the American Meteorological Society*, *98*(4), 681–698. https://doi.org/10.1175/BAMS-D-15-00230.1

Schmit, T. J., Gunshor, M. M., Menzel, W. P., Li, J., Bachmeier, S., & Gurka, J. J. (2005). Introducing the Next-generation Advanced Baseline Imager (ABI) on GOES-R. *Bulletin of the American Meteorological Society*, *86*, 1079–1096. https://doi.org/10.1175/BAMS-86-8-1079

Seemann, S. W., Borbas, E. E., Knuteson, R. O., Stephenson, G. R., & Huang, H.-L. (2008). Development of a global infrared land surface emissivity database for application to clear sky sounding retrievals from multi-spectral satellite radiance measurements. *Journal of Applied Meteorology and Climatology*, *47*(1), 108–123. https://doi.org/10.1175/2007JAMC1590.1

Shi, L., & Bates, J. J. (2011). Three decades of intersatellite calibrated High Resolution Infrared Radiation Sounder upper tropospheric water vapor. *Journal of Geophysical Research*, *116*, D04108. https://doi.org/10.1029/2010JD014847

Shi, L., Schreck, C. J. III, & John, V. O. (2012). An improved HIRS upper tropospheric water vapor dataset and its correlations with major climate indices. *Atmospheric Chemistry and Physics Discussions*, *12*(12), 33411–33442. https://doi.org/10.5194/acpd-12-33411-2012

Soden, B. J. (1998). Tracking upper tropospheric water vapor radiances: A satellite perspective. *Journal of Geophysical Research*, *103*(D14), 17,069–17,081. https://doi.org/10.1029/98JD01151

Tabata, T., John, V. O., Roebeling, R. A., Hewison, T., & Schulz, J. (2019). Re-calibration of over 35 years of infrared and water vapour channel radiances from the JMA geostationary satellites. *Remote Sensing*, *11*, 1189. https://www.mdpi.com/2072-4292/11/10/1189

Taylor, K. E., Stouffer, R. J., & Meehl, G. A. (2012). An Overview of CMIP5 and the Experiment Design. *Bulletin of the American Meteorological Society*, *93*, 485–498. https://doi.org/10.1175/BAMS-D-11-00094.1

Tian, Y., Huffman, G. J., Adler, R. F., Tang, L., Sapiano, M., Maggioni, V., & Wu, H. (2013). Modeling errors in daily precipitation measurements: Additive or multiplicative? *Geophysical Research Letters*, *40*, 2060–2065. https://doi.org/10.1002/grl.50320